Quasiparticle band gaps and optical spectra of strained monolayer transition-metal dichalcogenides

Wenshen Song and Li Yang

Phys. Rev. B **96**, 235441 — Published 26 December 2017

DOI: 10.1103/PhysRevB.96.235441

Quasiparticle Band Gaps and Optical Spectra of Strained Monolayer Transition Metal Dichalcogenides

Wenshen Song[1] and Li Yang[1, 2]

[1]Department of Physics, Washington University, Saint Louis, MO, 63130

[2]Institute of Materials Science and Engineering, Washington University in St. Louis, St. Louis, Missouri 63130, USA

Abstract

Employing the first-principles many-body perturbation theory, we report the excited-state properties, *i.e.*, quasiparticle energy and excitonic effects, of strained monolayer 2H-phase transition metal dichalcogenides, including MoS_2, $MoSe_2$, WS_2, and WSe_2. Beyond previous studies that considered uniaxial or biaxial strain, we cover arbitrarily axial strains and find complicated variations of quasiparticle band gaps, band edge energies, direct-indirect gap transitions, and exciton energies. These results provide a complete picture for straining engineering of electronic structures and optical spectra of two-dimensional transition metal dichalcogenides. Particularly, combined with high spatial-resolution optical measurements, our calculated results are essential for identifying local strain distribution and understanding the widely observed inhomogeneous free-carrier distributions and photoluminescence in realistic 2D materials.

Text

Strain is known for impacting a wide range of properties of semiconductors and thus it is useful to tailor materials for various applications [1-15]. This is particularly intriguing for two-dimensional (2D) structures that can sustain much larger magnitude of strain than their bulk counterparts. For example, significant strain effects have been observed in graphene and monolayer/few-layer transition metal dichalcogenides (TMDs) and they are useful for realizing a wide range of unique properties, such as pseudo-magnetism and photovoltaics [2, 16-19]. However, experimentally controllable strain engineering is still challenging. In particular, stretching or bending 2D structures usually introduces spatially inhomogeneous strain, as shown in schematics of Figure 1 (a). These complicated strain

distributions, which are beyond the scope of simple uniaxial or biaxial cases, will surely affect local electronic structures and optical properties, bringing uncertainty for strain engineering [1, 2, 20, 21]. Moreover, complicated strain distribution is widely expected in fabricated samples. Recently, the scalable production of 2D semiconductors, such as monolayer/few-layer TMDs, has achieved significant progresses [22-27]. Interestingly, those epitaxial samples exhibit various local properties: inhomogeneous free-carrier distributions and photoluminescence (PL) have been observed [28-30]. Given the important roles of substrates, edge reconstructions, and domain walls, strain may be inevitable in those fabricated samples [10, 31, 32]. In this sense, connecting optical or electrical inhomogeneity to spatial strain distributions is an effective way to understand these epitaxial processes and local structures, giving hope to further optimizing fabrications.

Other than experimental challenges, many questions still remain in theoretical studies in this field. Different from arbitrary or even inhomogeneous strain realized in experiments, most calculations have focused on relatively simple cases, such as uniaxial/biaxial strains along specific high-symmetry directions [33-35]. While uniaxial or biaxial strain decides many important properties, they are not enough for covering those experimentally strain conditions: the strain may be applied with differently amplitudes along different directions because of substrates or various boundary conditions, which are common in fabricated samples. Thus, a study covering arbitrarily axial strain is necessary and essential to explore the 2D strain-mapping properties [21, 36, 37], which is also important to fill a hole of previous studies. Moreover, typical *ab initio* calculations are based on density functional theory (DFT), but the aforementioned PL and band energies are essentially excited-state properties, requiring including many-electron effects, *i.e.*, electronic self-energy and electron-hole (*e*-*h*) interactions, which are beyond DFT. Therefore, a first-principles calculation considering complicated strain conditions and including many-electron effects is essential for explaining a wide range of measurements and guiding future strain engineering of 2D materials.

In this work, we apply the first-principles DFT and many-body perturbation theory (MBPT) to obtain quasiparticle energies and bright excitons of strained four typical TMD monolayers, *i.e.*, MoS_2, $MoSe_2$, WS_2, and WSe_2. By mapping their band gaps, absolute band edge energies, and exciton frequencies into 2D contours of in-plane strain distributions, we are able to provide a complete picture of arbitrary strain effects on these important quantities. Particularly, these strain-induced variations of the absolute band edge energies and exciton energies may accumulate optical excitations for light emission or photovoltaic applications. Combining the high spatial-resolution of PL spectra with our calculated exciton energies,

experimentalists may understand the observed inhomogeneous PL measurements and further quantify the local strain condition.

DFT with the Perdew–Burke–Ernzerhof (PBE) functional is employed to calculate the ground-state properties. Norm-conserving pseudopotentials are used to approximate the core-electron effects on the electronic structure and excited-state properties. Only the 2H phase is considered in this work and the atomic structure is fully relaxed according to the DFT/PBE-calculated force and stress. A 70 Ry plane-wave truncation and an 18x18x1 k-grid sampling in the first Brillouin Zone (BZ) of the intrinsic hexagonal unit cell are adopted for calculating fully converged ground-state properties. For strained calculations, we take a rectangle cell with 12×21×1 k-point. The quasiparticle energies are obtained by the first-principles single-shot G_0W_0 approximation [38] and subsequently excitonic effects and optical absorption spectra are obtained from solving the Bethe-Salpeter equation (BSE) within the Tam-Dancoff approximation [39]. The involved unoccupied band number is more than 10 times of that of valence bands to achieve the converged dielectric function. The excitonic effects are included by solving the BSE with a fine k-point grid of 36×63×1. The Coulomb truncation is implemented in GW-BSE calculations to mimic suspended monolayers [40, 41]. The convergence of overall quasiparticle band gaps and exciton energies are within 0.1 eV. We will employ the middle-gap approximation to identify the absolute quasiparticle band edge energy according to surrounding vacuum [42]. This can avoid a huge number of unoccupied conduction states in the GW calculations. Finally, we do not include extrinsic factors such as doping, substrate, and finite temperature effects, which, however, may impact quasiparticle band gaps and excitons [43-47].

Take monolayer MoS_2 as an example. Its intrinsic band structure calculated by DFT is presented in Figure 1 (b). The first BZ and those important high-symmetry points (including the Λ point) in the reciprocal space are plotted as well. Similar to previous studies [48], we observe a direct band gap located at the K (K') point in suspended monolayer MoS_2. Following the tradition, we define the two special in-plane orientations, the armchair and zigzag directions, which are marked in Figure 1 (a). In the following, beyond previously studied uniaxial/biaxial strain, we will include in-plane strain through a 2D grid, which is expanded by the orthogonal armchair and zigzag directions. The strain magnitude covers the range from -5% to 5% along each direction with a step of 0.5 %, forming a 21 x21 grid to describe strain conditions. The electronic structures and optical spectra will be calculated under each strain condition. As a result, this study covers not only uniaxial and biaxial strain cases but also all possible arbitrarily axial strain cases that are observed in fabricated samples. Finally, the linear interpolation scheme will be

employed to smooth the 2D contour plots. This procedure is similar to the recent works on Raman spectra of strained monolayer black phosphorus (BP) [49] and the band gap variation of strained bulk BP [9]. The local strain areas are typically of the μm order in MoS_2 samples[37] and the exciton size of MoS_2 is of the order of nm [50]. Therefore, it should be safe to assert that, in a local strain domain, excitons feel a constant strain and our calculations are realistic. In measurements, the recent spatial resolution of PL can reach 1 μm [29], making our calculation useful for experimental identification. However, if the resolution or the size of laser spots is larger than that of strain domains, the broadening of exciton peaks will be expected.

There are several factors that will influence our results. First, spin-orbit coupling (SOC) is significant in these monolayers. For example, the SOC splitting of the valence band maximum (VBM) of monolayer WS_2 is around 425 meV [51]. This will surely affect the band edge energies and excitons. Fortunately, we have checked that, although SOC is not negligible, it is not very sensitive to applied strain. For instance, the SOC splitting of the valence band edge at the K point is around 140 meV for monolayer MoS_2 and the variation of SOC is less than 10 meV when applied strain is within our studied range (+/- 5%). Thus, in the following we will directly include fixed SOC corrections into the band gaps and exciton energies for strained 2D structures.

Another challenge is to obtain the quasiparticle energies and excitons for strained structures. Because the GW-BSE calculation is much more time consuming than DFT, it is nearly formidable to perform the brute-force GW-BSE calculation for excited-state properties of the 21x21 strained structures. Fortunately, many-electron effects can be regarded as higher-order corrections. Therefore, although self-energy corrections and excitonic effects are significant, these many-electron corrections may not change substantially by strain within +/- 5%. To confirm this assumption, we have calculated the quasiparticle band gaps and optical spectra of intrinsic monolayer MoS_2 and two typical strained cases (+2% uniaxial and +2% biaxial cases), as included in table I and the figure 2. The SOC is not included here because we mainly want to compare the difference induced by strain and, moreover, SOC is not significantly changed by many-electron effects in these monolayers [52]. Substantial self-energy corrections and excitonic effects have been observed in all these monolayers. Our calculated quasiparticle band gap and optical absorption spectrum of intrinsic monolayer MoS_2 are consistent with previous studies [53, 54]. Importantly, many-electron corrections are essentially insensitive to the applied strain. For instance, the bright exciton peak of intrinsic monolayer MoS_2 is around 2.07 eV and the DFT band gap is around 1.69 eV. The overall energy difference is 0.38 eV. For the biaxial strain cases

(+2% along both the zigzag and armchair directions), the DFT band gap at the K point is reduced to be 1.47 eV while the bright exciton peak is also shifted to 1.86 eV, resulting in a similar 0.39 eV correction. Therefore, we only need to calculate the electronic self-energy corrections and excitonic effects of intrinsic materials. They are used to rigidly shift the quasiparticle bandgaps and excitonic energies of monolayer TMDs within moderate strain. To confirm this rigid shift, we have calculated more strain conditions. The error bar of the rigid shift is shown to be less than 0.1 eV, making it reasonable for applying rigid shifts to all quasiparticle band gaps and exciton energies. On the other hand, we must address that, although these rigid shifts do not bring new physics, they are necessary to be included in the final results because these energy values are essential for guiding experiments to identify the local strain via the measured band gaps or optical spectra. Finally, we are interested in the band gap that only involves the K point and the Γ point. Therefore, the k-point dependence of many-electron effects does not significantly affect our conclusions.

We first focus on excited-state properties of strained monolayer MoS_2. Its contour of the quasiparticle band gap with SOC included is presented in Figure 3 (a). Significant variations of the band gap are observed: within this +/- 5% strain range, the band gap can be changed from 1.7 eV to 2.8 eV (the intrinsic band gap is 2.6 eV). The band gap is particularly sensitive to both the magnitude of the applied strain and how the strain is applied. Interestingly, the most efficient way to tune the band gap is the widely studied one, the biaxial stretching. This can be seen from that the steepest sloping direction in figure 3 (a) is the along the diagonal direction (from the origin to the right-up corner). On the other hand, the biaxial strain effect is highly asymmetric: the band gap is not changed substantially for the compressing case. This is actually a result of switching band edges, which will be discussed later.

On the other hand, as shown in figure 3 (a), along the orthogonal direction to the biaxial strain, the band gap variation is, however, the minimum. For instance, for the strain condition marked by a blue cross in Figure 3 (a), which is a combination of +3% zigzag strain and -3% armchair strain, the band gap is nearly the same as the intrinsic value. Based on those isolines in Figure 3 (a), we can conclude that when the 2D structure is stretched along one direction and compressed along the other orthogonal direction, its variation of the band gap is small. In other words, the conservation of the in-plane area can minimize the band-gap variation in strained TMDs.

In addition to the band gap value, the direct/indirect band gap is a crucial parameter in semiconductors because it decides the transport and optical properties of semiconductors. Previous studies predicted this transition for uniaxial (armchair/zigzag) strain in monolayer TMDs [55, 56]. In Figure 3 (a), we

present a complete picture of strain effect for such a direct-indirect band-gap transition in monolayer MoS_2. The grey area stands for the strain condition for holding a direct-band gap and the white area stands for that of an indirect band gap. Particularly, Figure 3 (a) shows that even under significant stretch along one direction, monolayer TMDs may still hole the direct band gap if it is allowed for shrinking along the orthogonal direction, e.g., the blue cross.

The above direct-indirect band-gap transitions are essentially from the competitions between band edges at those high-symmetry points, marked in Figure 1 (b). In Figures 3 (b), we have plotted the three-dimensional (3D) contour plot of the absolute quasiparticle energies of the valence and conduction band edges of those relevant high-symmetry points, according to the vacuum level. We can see that there are energy crossings between those band edges. For example, in figure 3 (b), under the biaxial stretch, the local valence band maximum (VBM) at the Γ point increases while that at the K point decreases. As a result, above a critical stretch, the VBM is shifted from the K point to the Γ point, inducing a direct-indirect band gap transition. The similar conclusion can be drawn for the conduction band minimum (CBM). As shown Figure 3 (b), the local minimum at the Λ point is nearly insensitive to the applied strain while that at the K point is very sensitive. Therefore, under compress strain, we see that the local minimum at the K point quickly increases and the band edge at the Λ point becomes the new CBM, resulting in an indirect band gap.

It is important to understand the different strain responses of these band edges at high-symmetry points. A full description can be obtained by the well-established tight-binding model [57], in which the hopping parameters between different orbitals can be quantified. Here, we use a schematic way to qualitatively understand these different strain responses. As an example, we focus on that the local conduction band minimum at the Λ and K points. We have plotted the three-dimensional (3D) isosurface plots of their wavefunctions in figure 3 (c). The electronic state at the Λ point is more localized and the overlap between neighboring unit cells is small. On the other hand, the wavefunction at the K point is more delocalized and has a significant overlap between neighboring unit cells. Then under strain, the lightly overlapped wave function at the Λ point will not be that sensitive to the change of in-plane distance between atoms, compared to the strongly overlapped state at the K point. This is also consistence with the results in Figure 3 (b), in which the energy of the state at the Λ pointy is nearly fixed while that of the state at the K point is varied substantially according to strain.

This arbitrary strain effect on the absolute band edge energies is useful for understanding the recently observed inhomogeneous carrier density in monolayer TMDCs [28, 30]. Due to the substrate effect or

ripple structures, those samples may have inevitable locally complicated strain distributions, which may be neither uniaxial nor biaxial. In particular, for those triangular-shape samples epitaxially growing on SiO_2/Si substrate, the strain may be accumulated at the corners or edges, inducing a significant shift of the absolute band edge energy and subsequent inhomogeneous free-carrier distributions [29]. For example, according to figure 3 (b), the accumulations of electrons or holes may indicate a locally biaxial stretching strain condition because that strain condition can efficiently decrease the CBM of increase the VBM.

Finally, the GW-BSE calculated energies of the brightest exciton in all four types of monolayer 2H-phase TMDs, i.e., MoS_2, $MoSe_2$, WS_2, and WSe_2, according to arbitrarily axial strain are presented in Figures 4. From these 2D contour plots, we can see that strain can significantly modify the PL frequency. Importantly, within our strain range (+/- 5%), the optical response edge can be tuned from the visible light range to the near infrared one (~1.3 eV). This will be useful for broad physics and biological applications [58]. Meanwhile, the PL peak is strongly impacted by the direct/indirect band gap and it is expected that the PL intensity will be substantially quenched for those indirect band gap regions. Therefore, we mark the direct-indirect band gap transition regimes in figure 4 to guide strain engineering for optical applications. Monolayer $MoSe_2$ seems to be the most robust direct-gap TMD under stain. It can hold the direct band-gap exciton for compress strain up to 1.5% or the stretching strain up to 3.5%. On the contrary, intrinsic monolayer WSe_2 is almost an indirect band-gap 2D semiconductors. Interestingly, it is always an indirect-gap semiconductor under compress and a direct-gap one under stretch.

The exciton energy according to complicated strain in Figure 4 is useful to understand recent optical measurements. To date the techniques for obtaining PL spectra with a high spatial resolution has been highly developed and applied for studying epitaxially grown samples [29]. In addition to the inhomogeneous carrier distributions, the local strain condition may also be responsible for the shift of the frequency of the PL peak with a spatial resolution. Therefore, our results in Figure 4 will be of help to understand the local strain distribution. Moreover, combined with the strain induced the variation of the band edge energy and exciton energy, it is possible to design strain distribution to accumulate optically excited excitons and realize high-efficient light-emission or photovoltaic devices [59].

In conclusion, we have presented excited-state properties, including absolute quasiparticle band energies, band gaps, and the bright exciton peak, for arbitrarily in-plane strain of typical monolayer 2H-phase TMDCs. With many-electron effects include, the complete pictures of these important quantities

are described by 2D contours of strain conditions. The mechanism for the competition of band edge energies and its impact on band gaps are discussed based on first-principles results. The variations of these quantities are crucial for experiments to understand local strain distribution and free-carrier inhomogeneity by optical measurements. The predicted arbitrary strain effects are also helpful for strain engineering of transport and optical properties.

We are supported by the National Science Foundation (NSF) Grant No. DMR-1207141 and NSF CAREER Grant No. DMR-1455346. The ground state calculation is performed by quantum espresso [60]. The GW–BSE calculation is done with the BerkeleyGW package [61]. This work used the Extreme Science and Engineering Discovery Environment (XSEDE), which is supported by National Science Foundation grant number ACI-1548562.

[1] K. Liu, Q. Yan, M. Chen, W. Fan, Y. Sun, J. Suh, D. Fu, S. Lee, J. Zhou, S. Tongay, Elastic properties of chemical-vapor-deposited monolayer MoS2, WS2, and their bilayer heterostructures, Nano Lett. 14, 5097 (2014).
[2] S. Bertolazzi, J. Brivio, A. Kis, Stretching and breaking of ultrathin MoS2, ACS nano 5, 9703 (2011).
[3] M.R. Falvo, G. Clary, R. Taylor Ii, V. Chi, Bending and buckling of carbon nanotubes under large strain, Nature 389, 582 (1997).
[4] M. Fischetti, Z. Ren, P. Solomon, M. Yang, K. Rim, Six-band k· p calculation of the hole mobility in silicon inversion layers: Dependence on surface orientation, strain, and silicon thickness, J. Appl. Phys. 94, 1079 (2003).
[5] J. Haeni, P. Irvin, W. Chang, R. Uecker, Room-temperature ferroelectricity in strained SrTiO3, Nature 430, 758 (2004).
[6] R.S. Jacobsen, K.N. Andersen, P.I. Borel, J. Fage-Pedersen, L.H. Frandsen, O. Hansen, M. Kristensen, A.V. Lavrinenko, G. Moulin, H. Ou, Strained silicon as a new electro-optic material, Nature 441, 199 (2006).
[7] K. Lai, M. Nakamura, W. Kundhikanjana, M. Kawasaki, Y. Tokura, M.A. Kelly, Z.-X. Shen, Mesoscopic percolating resistance network in a strained manganite thin film, Science 329, 190 (2010).
[8] R. Fei, L. Yang, Strain-engineering the anisotropic electrical conductance of few-layer black phosphorus, Nano Lett. 14, 2884 (2014).
[9] J. Guan, W. Song, L. Yang, D. Tománek, Strain-controlled fundamental gap and structure of bulk black phosphorus, Phys. Rev. B 94, 045414 (2016).
[10] H.J. Conley, B. Wang, J.I. Ziegler, R.F. Haglund Jr, S.T. Pantelides, K.I. Bolotin, Bandgap engineering of strained monolayer and bilayer MoS2, Nano Lett. 13, 3626 (2013).
[11] W.S. Yun, S. Han, S.C. Hong, I.G. Kim, J. Lee, Thickness and strain effects on electronic structures of transition metal dichalcogenides: 2H-M X 2 semiconductors (M= Mo, W; X= S, Se, Te), Phys. Rev. B 85, 033305 (2012).
[12] L. Yang, X. Cui, J. Zhang, K. Wang, M. Shen, S. Zeng, S.A. Dayeh, L. Feng, B. Xiang, Lattice strain effects on the optical properties of MoS2 nanosheets, Sci. Rep. 4, 5649 (2014).
[13] Z.H. Ni, T. Yu, Y.H. Lu, Y.Y. Wang, Y.P. Feng, Z.X. Shen, Uniaxial Strain on Graphene: Raman Spectroscopy Study and Band-Gap Opening, ACS Nano 2, 483 (2009).

[14] H. Pan, Y.-W. Zhang, Tuning the electronic and magnetic properties of MoS2 nanoribbons by strain engineering, J. Phys. Chem. C 116, 11752 (2012).
[15] L. Kou, C. Tang, Y. Zhang, T. Heine, C. Chen, T. Frauenheim, Tuning magnetism and electronic phase transitions by strain and electric field in zigzag MoS2 nanoribbons, J. Phys. Chem. Lett. 3, 2934 (2012).
[16] C. Lee, X. Wei, J.W. Kysar, J. Hone, Measurement of the elastic properties and intrinsic strength of monolayer graphene, Science 321, 385 (2008).
[17] F. Guinea, M. Katsnelson, A. Geim, Energy gaps and a zero-field quantum Hall effect in graphene by strain engineering, Nat. Phys. 6, 30 (2010).
[18] M. Bernardi, M. Palummo, J.C. Grossman, Extraordinary sunlight absorption and one nanometer thick photovoltaics using two-dimensional monolayer materials, Nano Lett. 13, 3664 (2013).
[19] M.-L. Tsai, S.-H. Su, J.-K. Chang, D.-S. Tsai, C.-H. Chen, C.-I. Wu, L.-J. Li, L.-J. Chen, J.-H. He, Monolayer MoS2 heterojunction solar cells, ACS nano 8, 8317 (2014).
[20] G.-H. Lee, Y.-J. Yu, X. Cui, N. Petrone, C.-H. Lee, M.S. Choi, D.-Y. Lee, C. Lee, W.J. Yoo, K. Watanabe, Flexible and transparent MoS2 field-effect transistors on hexagonal boron nitride-graphene heterostructures, ACS nano 7, 7931 (2013).
[21] M. Mehboudi, K. Utt, H. Terrones, E.O. Harriss, A.A.P. SanJuan, S. Barraza-Lopez, Strain and the optoelectronic properties of nonplanar phosphorene monolayers, Proc. Natl. Acad. Sci. U.S.A. 112, 5888 (2015).
[22] Y. Xue, Y. Zhang, Y. Liu, H. Liu, J. Song, J. Sophia, J. Liu, Z. Xu, Q. Xu, Z. Wang, Scalable production of a few-layer MoS2/WS2 vertical heterojunction array and its application for photodetectors, ACS nano 10, 573 (2015).
[23] Y. Shi, W. Zhou, A.-Y. Lu, W. Fang, Y.-H. Lee, A.L. Hsu, S.M. Kim, K.K. Kim, H.Y. Yang, L.-J. Li, van der Waals epitaxy of MoS2 layers using graphene as growth templates, Nano Lett. 12, 2784 (2012).
[24] D. Dumcenco, D. Ovchinnikov, K. Marinov, P. Lazić, M. Gibertini, N. Marzari, O.L. Sanchez, Y.-C. Kung, D. Krasnozhon, M.-W. Chen, Large-area epitaxial monolayer MoS2, ACS Nano 9, 4611 (2015).
[25] K.F. Mak, K. He, J. Shan, T.F. Heinz, Control of valley polarization in monolayer MoS2 by optical helicity, Nat. Nanotech. 7, 494 (2012).
[26] O. Lopez-Sanchez, D. Lembke, M. Kayci, A. Radenovic, A. Kis, Ultrasensitive photodetectors based on monolayer MoS2, Nat. Nanotech. 8, 497 (2013).
[27] H. Li, Q. Zhang, C.C.R. Yap, B.K. Tay, T.H.T. Edwin, A. Olivier, D. Baillargeat, From bulk to monolayer MoS2: evolution of Raman scattering, Adv. Funct. Mater. 22, 1385 (2012).
[28] A. Singh, G. Moody, K. Tran, M.E. Scott, V. Overbeck, G. Berghäuser, J. Schaibley, E.J. Seifert, D. Pleskot, N.M. Gabor, Trion formation dynamics in monolayer transition metal dichalcogenides, Phys. Rev. B 93, 041401 (2016).
[29] N.J. Borys, E.S. Barnard, S. Gao, K. Yao, W. Bao, A. Buyanin, Y. Zhang, S. Tongay, C. Ko, J. Suh, Anomalous Above-Gap Photoexcitations and Optical Signatures of Localized Charge Puddles in Monolayer Molybdenum Disulfide, ACS nano 11, 2115 (2017).
[30] T. Jakubczyk, V. Delmonte, M. Koperski, K. Nogajewski, C. Faugeras, W. Langbein, M. Potemski, J. Kasprzak, Radiatively limited dephasing and exciton dynamics in MoSe2 monolayers revealed with four-wave mixing microscopy, Nano Lett. 16, 5333 (2016).
[31] A. Castellanos-Gomez, R. Roldán, E. Cappelluti, M. Buscema, F. Guinea, H.S. van der Zant, G.A. Steele, Local strain engineering in atomically thin MoS2, Nano Lett. 13, 5361 (2013).
[32] K. He, C. Poole, K.F. Mak, J. Shan, Experimental demonstration of continuous electronic structure tuning via strain in atomically thin MoS2, Nano Lett. 13, 2931 (2013).
[33] X. Wei, B. Fragneaud, C.A. Marianetti, J.W. Kysar, Nonlinear elastic behavior of graphene: Ab initio calculations to continuum description, Phys. Rev. B 80, 205407 (2009).
[34] F. Liu, P. Ming, J. Li, Ab initio calculation of ideal strength and phonon instability of graphene under tension, Phys. Rev. B 76, 064120 (2007).

[35] P. Johari, V.B. Shenoy, Tuning the electronic properties of semiconducting transition metal dichalcogenides by applying mechanical strains, ACS nano 6, 5449 (2012).
[36] A. Armigliato, R. Balboni, G. Carnevale, G. Pavia, D. Piccolo, S. Frabboni, A. Benedetti, A. Cullis, Application of convergent beam electron diffraction to two-dimensional strain mapping in silicon devices, Appl. Phys. Lett. 82, 2172 (2003).
[37] Z. Liu, M. Amani, S. Najmaei, Q. Xu, X. Zou, W. Zhou, T. Yu, C. Qiu, A.G. Birdwell, F.J. Crowne, Strain and structure heterogeneity in MoS2 atomic layers grown by chemical vapour deposition, Nat. Commun. 5, 5246 (2014).
[38] M.S. Hybertsen, S.G. Louie, Electron correlation in semiconductors and insulators: Band gaps and quasiparticle energies, Phys. Rev. B 34, 5390 (1986).
[39] M. Rohlfing, S.G. Louie, Electron-hole excitations and optical spectra from first principles, Phys. Rev. B 62, 4927 (2000).
[40] S. Ismail-Beigi, Truncation of periodic image interactions for confined systems, Phys. Rev. B 73, 233103 (2006).
[41] C.A. Rozzi, D. Varsano, A. Marini, E.K. Gross, A. Rubio, Exact Coulomb cutoff technique for supercell calculations, Phys. Rev. B 73, 205119 (2006).
[42] Y. Liang, S. Huang, R. Soklaski, L. Yang, Quasiparticle band-edge energy and band offsets of monolayer of molybdenum and tungsten chalcogenides, Appl. Phys. Lett. 103, 042106 (2013).
[43] Y. Liang, L. Yang, Carrier plasmon induced nonlinear band gap renormalization in two-dimensional semiconductors, Phys. Rev. Lett. 114, 063001 (2015).
[44] S. Gao, Y. Liang, C.D. Spataru, L. Yang, Dynamical excitonic effects in doped two-dimensional semiconductors, Nano Lett. 16, 5568 (2016).
[45] R. Soklaski, Y. Liang, L. Yang, Temperature effect on optical spectra of monolayer molybdenum disulfide, Appl. Phys. Lett. 104, 193110 (2014).
[46] C. Zhang, H. Wang, W. Chan, C. Manolatou, F. Rana, Absorption of light by excitons and trions in monolayers of metal dichalcogenide Mo S 2: Experiments and theory, Phys. Rev. B 89, 205436 (2014).
[47] M.M. Ugeda, A.J. Bradley, S.-F. Shi, F.H. da Jornada, Y. Zhang, D.Y. Qiu, W. Ruan, S.-K. Mo, Z. Hussain, Z.-X. Shen, F. Wang, S.G. Louie, M.F. Crommie, Giant bandgap renormalization and excitonic effects in a monolayer transition metal dichalcogenide semiconductor, Nat. Mater. 13, 1091 (2014).
[48] A. Splendiani, L. Sun, Y. Zhang, T. Li, J. Kim, C.-Y. Chim, G. Galli, F. Wang, Emerging photoluminescence in monolayer MoS2, Nano Lett. 10, 1271 (2010).
[49] R. Fei, L. Yang, Lattice vibrational modes and Raman scattering spectra of strained phosphorene, Appl. Phys. Lett. 105, 083120 (2014).
[50] Y. Yu, Y. Yu, Y. Cai, W. Li, A. Gurarslan, H. Peelaers, D.E. Aspnes, C.G. Van de Walle, N.V. Nguyen, Y.-W. Zhang, Exciton-dominated dielectric function of atomically thin MoS2 films, Sci. Rep. 5, (2015).
[51] D.W. Latzke, W. Zhang, A. Suslu, T.-R. Chang, H. Lin, H.-T. Jeng, S. Tongay, J. Wu, A. Bansil, A. Lanzara, Electronic structure, spin-orbit coupling, and interlayer interaction in bulk MoS 2 and WS 2, Phys. Rev. B 91, 235202 (2015).
[52] B.D. Malone, M.L. Cohen, Quasiparticle semiconductor band structures including spin–orbit interactions, J. Phys.: Condens. Matter 25, 105503 (2013).
[53] A. Ramasubramaniam, Large excitonic effects in monolayers of molybdenum and tungsten dichalcogenides, Phys. Rev. B 86, 115409 (2012).
[54] D.Y. Qiu, H. Felipe, S.G. Louie, Optical spectrum of MoS 2: many-body effects and diversity of exciton states, Phys. Rev. Lett. 111, 216805 (2013).
[55] E. Scalise, M. Houssa, G. Pourtois, V. Afanas'ev, A. Stesmans, Strain-induced semiconductor to metal transition in the two-dimensional honeycomb structure of MoS2, Nano Res. 5, 43 (2012).
[56] J.K. Ellis, M.J. Lucero, G.E. Scuseria, The indirect to direct band gap transition in multilayered MoS2 as predicted by screened hybrid density functional theory, Appl. Phys. Lett. 99, 261908 (2011).

[57] E. Cappelluti, R. Roldán, J. Silva-Guillén, P. Ordejón, F. Guinea, Tight-binding model and direct-gap/indirect-gap transition in single-layer and multilayer MoS 2, Phys. Rev. B 88, 075409 (2013).
[58] A.M. Smith, M.C. Mancini, S. Nie, Bioimaging: second window for in vivo imaging, Nat. Nanotech. 4, 710 (2009).
[59] J. Feng, X. Qian, C.-W. Huang, J. Li, Strain-engineered artificial atom as a broad-spectrum solar energy funnel, Nat. Photon. 6, 866 (2012).
[60] P. Giannozzi, S. Baroni, N. Bonini, M. Calandra, R. Car, C. Cavazzoni, D. Ceresoli, G.L. Chiarotti, M. Cococcioni, I. Dabo, QUANTUM ESPRESSO: a modular and open-source software project for quantum simulations of materials, J. Phys.: Condens. Matter 21, 395502 (2009).
[61] J. Deslippe, G. Samsonidze, D.A. Strubbe, M. Jain, M.L. Cohen, S.G. Louie, BerkeleyGW: A massively parallel computer package for the calculation of the quasiparticle and optical properties of materials and nanostructures, Comput. Phys. Commun. 183, 1269 (2012).

Figures:

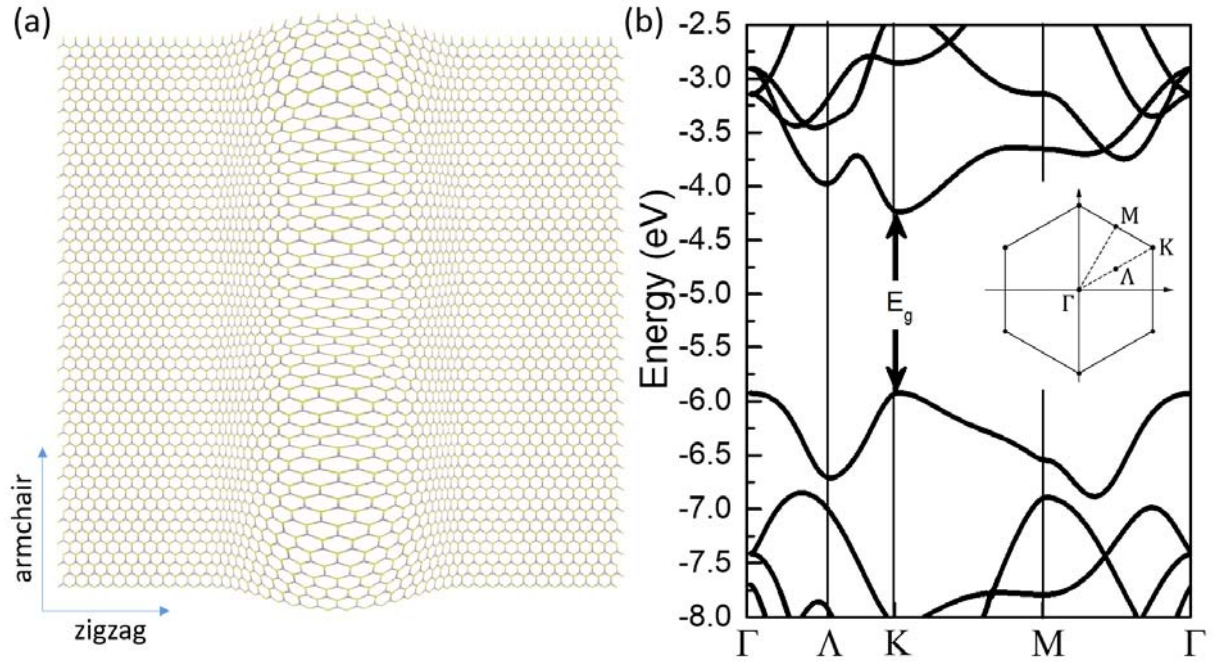

Figure 1 (a) A schematic plot of the top view of inhomogeneously strained monolayer 2-H phase TMD. The orthogonal armchair and zigzag directions are specified, respectively. To show atomic structures, the spatial size of plotted local strain domains is much smaller than that of realistic samples, which is around microns. (b) The DFT-calculated band structure of monolayer MoS_2. The band energy is aligned to the vacuum level. The inset is the first BZ with high-symmetry points marked.

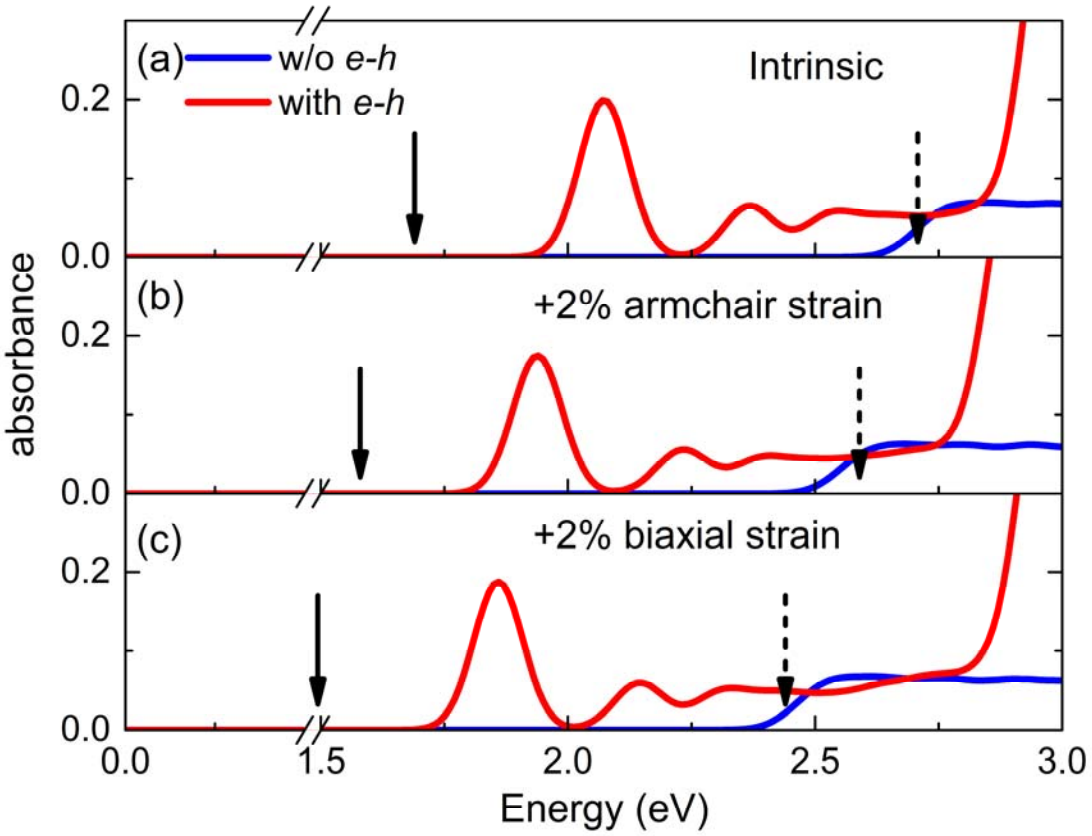

Figure 2 (a), (b), and (c) optical absorption spectra of intrinsic, +2% uniaxially strained, and +2% biaxially strained monolayer MoS_2. The blue curves are optical absorption spectra without *e-h* interactions included and the red curves are those with *e-h* interactions included. The DFT band gap (E_g^{DFT}) and GW calculated quasiparticle band gap (E_g^{GW}) are marked with solid and dash arrow, respectively.

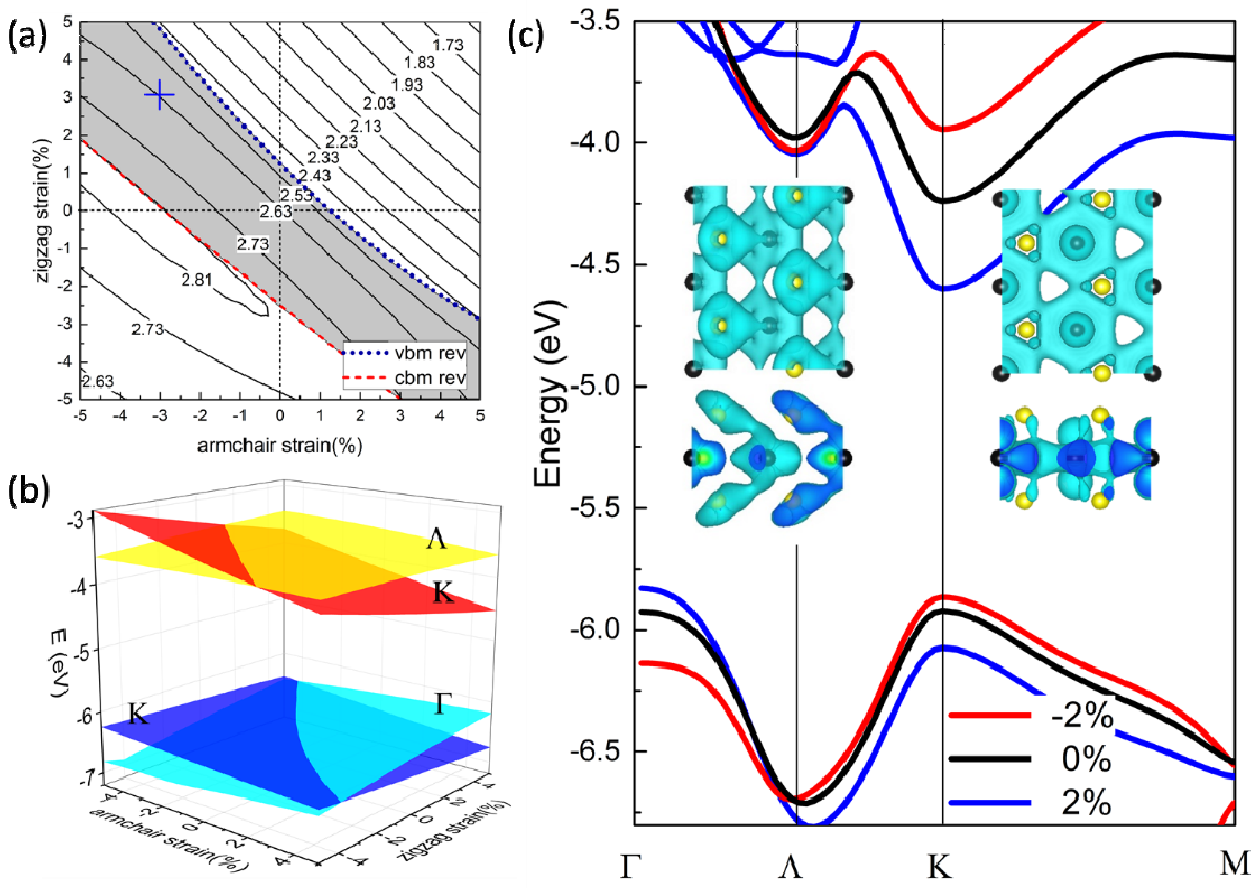

Figure 3 (a) 2D contour plot of the quasiparticle band gap in arbitrarily strained monolayer MoS_2. The indirect band-gap area is marked by the grey color. (b) The 3D contour plot of the absolute band energies of those crucial high-symmetry points. (c) The variation of the band structure according to the +/- 2% biaxial strain. The top view and side view of the 3D contours of the wave functions of the conduction states at the Λ and K points are plotted, respectively.

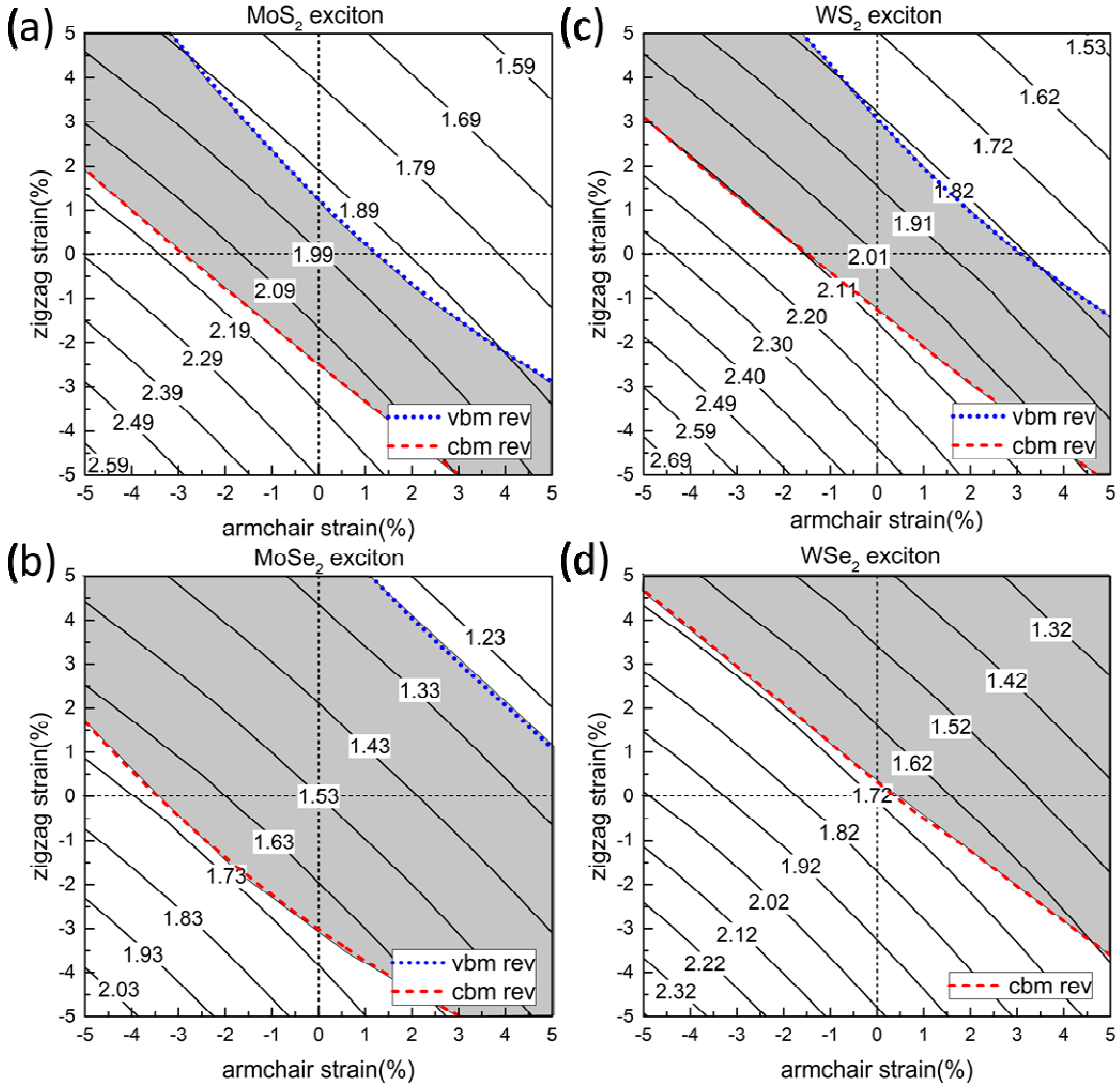

Figure 4 Contour plots of the excitation energy of the lowest-energy bright exciton of strained monolayer MoS_2 (a), WS_2 (b), $MoSe_2$ (c) and WSe_2 (d). The direct band-gap regions are marked by the grey area. SOC is approximately included as a constant correction. The temperature effect is not included.

Tables

Table I The DFT calculated band gaps (at the K point), quasiparticle band gaps (at the K point), and the lowest, bright exciton energies intrinsic and strained monolayer MoS_2 (SOC is not included).

Strain	DFT (eV)	GW (eV)	Exciton (eV)
Intrinsic	1.69	2.71	2.07
+2% armchair	1.58	2.59	1.94
+2% biaxial	1.47	2.44	1.86